Energy cascade and the four-fifths law in superfluid turbulence

Julien Salort, Benoît Chabaud, Emmanuel Lévêque, Philippe-Emmanuel Roche

epl 2012 (in press)

Energy cascade and the four-fifths law in superfluid turbulence

J. Salort[1], B. Chabaud[1], E. Lévêque[2] and P.-E. Roche[1]

[1] *Institut Néel, CNRS/UJF - BP 166, F-38042 Grenoble cedex 9, France, EU*
[2] *Laboratoire de Physique de l'ENS de Lyon, CNRS/Université Lyon, F-69364 Lyon cedex 7, France, EU*

PACS 47.37.+q – Hydrodynamic aspects of superfluidity; quantum fluids
PACS 67.57.De – Superflow and hydrodynamics
PACS 67.25.dk – Vortices and turbulence

Abstract –The 4/5-law of turbulence, which characterizes the energy cascade from large to small-sized eddies at high Reynolds numbers in classical fluids, is verified experimentally in a superfluid ^{4}He wind tunnel, operated down to 1.56 K and up to $R_\lambda \approx 1640$. The result is corroborated by high-resolution simulations of Landau-Tisza's two-fluid model down to 1.15 K, corresponding to a residual normal fluid concentration below 3 % but with a lower Reynolds number of order $R_\lambda \approx 100$. Although the Kármán-Howarth equation (including a viscous term) is not valid *a priori* in a superfluid, it is found that it provides an empirical description of the deviation from the ideal 4/5-law at small scales and allows us to identify an effective viscosity for the superfluid, whose value matches the kinematic viscosity of the normal fluid regardless of its concentration.

Introduction. – At low temperature, but above the so-called *lambda* transition, liquid ^{4}He is a classical fluid known as He I. Like air or water, its dynamics obeys the Navier-Stokes equation. When such a fluid is strongly stirred, its response is dominated by the non-linearity of the Navier-Stokes equation. The dynamics of such a system, known as "turbulence", was first pictured by Richardson in 1920 and theorized by Kolmogorov in 1941 [1]. The kinetic energy, injected at some large scales, cascades down across the so-called *inertial* scales until it reaches the dissipative scales. It can be derived from the Navier-Stokes equation that this energy flux across scales results in skewed distributions for the velocity increments. This prediction (the only exact result known for turbulence) is sometimes referred to as the Kolmogorov's 4/5-law. It is recalled later in this paper.

When liquid ^{4}He is cooled below $T_\lambda \approx 2.17$ K (at saturated vapor pressure), it undergoes the lambda phase transition. The new phase, called He II, can be described within the so-called *two-fluid model* [2], *i.e.* the superposition of a viscous "normal fluid" and an inviscid "superfluid" with quantized vorticity, these two components being coupled by a mutual friction term. The fraction ρ_s/ρ_n — where ρ_s and ρ_n are respectively the densities of the superfluid and normal components — varies with temperature from 0, at T_λ, to ∞ in the zero-temperature limit. When He II is strongly stirred, a tangle of quantum vortices is generated. This type of turbulent flow is characterized as "quantum turbulence" or "superfluid turbulence". For an introduction to quantum turbulence, one may refer to [3, 4].

The focus of this letter is on intense turbulence in He II at finite temperature, *i.e.* $T_\lambda > T \geq 1$ K. In such conditions, most of the superfluid kinetic energy distributes itself between the mechanical-forcing scale (at $\sim$1 cm in [5]) and the inter-vortex scale (at $\sim$4 µm in [5]). Excitations at smaller scales are strongly damped by the viscosity of the normal component [3]. At scales larger than the inter-vortex spacing the details of individual vortices are smoothed out ("continuous" or "coarse-grained" description) and superfluid turbulence can be investigated with the same statistical tools as classical turbulence. An important open question is how superfluid turbulence compares with classical turbulence. Experimental studies have revealed differences regarding vorticity spectra [5, 6] but also striking similarities concerning decay-rate scaling [7–10], drag force [11–13] and $k^{-5/3}$ scaling for the energy spectrum [14, 15]. This latter is consistent with the existence of an energy cascade (as described by Kolmogorov's theory), however no direct proof has been reported yet, as stressed recently during the *Quantum Turbulence Workshop* in Abu Dhabi [16] (see also the conclusion of [17]).

The main goal of this paper is to test in superfluid turbulence the characteristic 4/5-law of the energy cascade. To account for departure from the ideal 4/5-law at small scales, the classical Kármán-Howarth equation is assessed. As a side result, it is showed that the superfluid inherits viscosity from the normal component even when the normal fraction is very low, therefore making the velocity signal of a superfluid (obtained by an inertial anemome-

ter like a Pitot tube) hardly distinguishable from the one of a classical fluid.We consider experimental velocity fluctuations measurements obtained in a 1 m-long cryogenic helium wind tunnel at high Reynolds number, as well as results from direct numerical simulations of the continuous two-fluid model, at lower Reynolds numbers but fully resolved down to the mean inter-vortex scale.

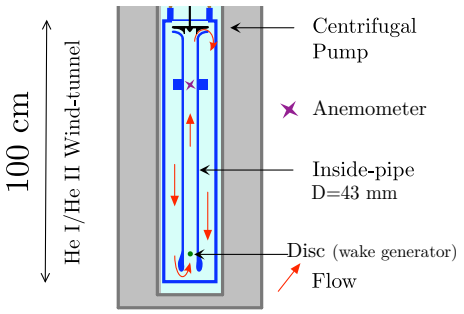

Fig. 1: Wind tunnel (in blue) in the cryostat (in gray)

Local velocity measurements. – Local velocity measurements have been performed in the far wake of a disc in the wind tunnel sketched in figure 1. The disc diameter $\varnothing_d$ is half the pipe diameter. The probe, located downstream at $x/\varnothing_d \approx 21$, was operated both above and below the superfluid transition, down to 1.56 K for which $\rho_s/\rho_n \approx 5.8$. The wind tunnel is pressurized by more than 1 m of static liquid to prevent cavitation. The turbulence intensity, $\tau = \sqrt{\langle (v(t) - \langle v \rangle)^2 \rangle}/\langle v \rangle$, where $v(t)$ is the local flow velocity and $\langle . \rangle$ stands for time average, is close to 4.8 %; the mean velocity is $\langle v \rangle = 1\,\mathrm{m/s}$. The forcing length scale, L_0, is obtained from the frequency of vortex shedding: $f_0 = \langle v \rangle / L_0$. This latter is estimated from the velocity spectrum (see figure 2). The typical Strouhal number

$$St = \frac{f_0 \varnothing_d}{\langle v \rangle} = \frac{\varnothing_d}{L_0} \tag{1}$$

is found close to 0.35 both above and below the superfluid transition. At $T = 2.2\,\mathrm{K}$, where liquid helium is a classical fluid with kinematic viscosity $\nu = 1.78 \times 10^{-8}\,\mathrm{m^2/s}$ [18], the Reynolds number $Re = v_{\mathrm{rms}} L_0/\nu = 1.8 \times 10^5$. The Reynolds number based on Taylor microscale is here approximated by $R_\lambda = \sqrt{15\,Re} \approx 1640$.

The local anemometer is the probe labeled as ① in [15]. It is based on a stagnation pressure measurement (miniature "Pitot tube" probe). It measures the pressure overhead resulting from the stagnation point at the tip of the probe, which is pointing upflow. Above the superfluid transition, the measured pressure $p_{\mathrm{meas}}(t)$ is

$$p_{\mathrm{meas}}(t) = p(t) + \frac{1}{2}\rho v^2 \tag{2}$$

Following [14], a similar expression can be found for the measured pressure below the lambda transition using the continuous two-fluid description of He II:

$$p_{\mathrm{meas}}(t) = p(t) + \frac{1}{2}\rho_n v_n^2 + \frac{1}{2}\rho_s v_s^2 \tag{3}$$

where v_n is the velocity of the normal component and v_s is the velocity of the superfluid component. Yet, physically, the probe is sensitive to the flux of momentum on its tip. It is therefore convenient [19] to rewrite the measured pressure in terms of the "momentum velocity", $\vec{v}_m$, with

$$\rho \vec{v}_m = \rho_n \vec{v}_n + \rho_s \vec{v}_s \tag{4}$$

where $\rho = \rho_n + \rho_s$. This leads to

$$p_{\mathrm{meas}}(t) = p(t) + \frac{1}{2}\rho v_m^2 + \frac{\rho_n \rho_s}{2\rho}\left(v_n - v_s\right)^2 \tag{5}$$

This equation is similar to the one standing in classical fluid (Eq. 2) except for an additional term. It has been argued theoretically [3] and shown numerically [20] that, in the fully-developed turbulent regime, the normal and superfluid components are nearly locked at inertial scales. Therefore, $(v_n - v_s)^2 \ll v_m^2$ and since $\rho_n \rho_s \leq \rho^2$, the last term in Eq. 5 can be neglected[1].

The calibrations of the probe above and below the superfluid transition are consistent with each other within 10 %. Discrepancies come mainly from experimental uncertainties. In practice, the calibration obtained below T_λ, where the signal is cleaner, was used to determine the mean values obtained in normal fluid. A numerical 4^{th}-order Butterworth low-pass filter is applied to the velocity time series to suppress the probe organ-pipe resonance [15]. The filtered velocity time series are converted into spatial signals using the instantaneous Taylor's frozen turbulence hypothesis [21], *i.e.* the velocity at location x is mapped to the velocity at time t, so that

$$v(x) = v(t) \text{ with } x = \int_0^t v(\tau)\mathrm{d}\tau \tag{6}$$

Velocity power spectra and probability distribution functions (PDF) are estimated from velocity series recast in space, $v(x)$, and shown in figure 2. As expected, power spectra exhibit a Kolmogorov's $k^{-5/3}$ scaling and the velocity PDF is nearly Gaussian. The spectra above and below the superfluid transition are found nearly identical. The wave number are normalized by the forcing scale L_0 (see above). Let us mention that the observed cut-off at high k results from the finite resolution of the probes and not from a dissipative effect.

The longitudinal velocity increments, here along the streamwise direction, are defined as

$$\delta v(x; r) = v(x + r) - v(x) \tag{7}$$

The PDF of $\delta v(x; r)$ for a given separation r is shown in figure 3. It is fairly Gaussian at large scale ($r \approx L_0$) and clearly skewed on the negative side at smaller scales

[1] When the turbulence intensity τ is small, the same approximation is obtained with the weaker hypothesis: $\langle v_s \rangle = \langle v_n \rangle$, *i.e.* the normal and superfluid components are locked at large scales [19]. The additional term is of order τ^2 at most, and can be neglected.

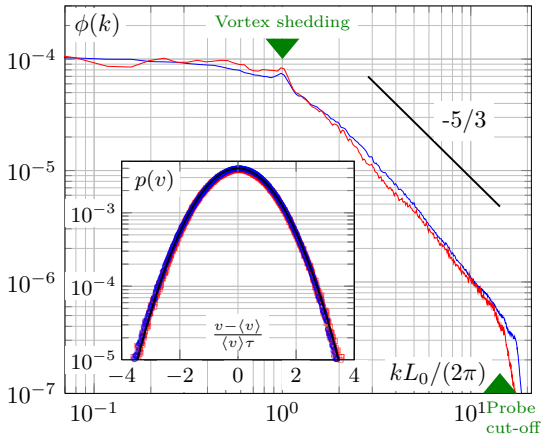

Fig. 2: Experimental 1D velocity power spectrum above and below the superfluid transition. Red line: $T = 2.2\,\mathrm{K} > T_\lambda$ at $R_\lambda \approx 1640$. Blue line: $T = 1.56\,\mathrm{K} < T_\lambda$. Inset: Velocity probability density distribution above and below the superfluid transition. Black line: Gaussian distribution.

($r \approx L_0/10$). The skewness $S(r)$ is defined as

$$S(r) = \frac{\langle \delta v(r)^3 \rangle}{\langle \delta v(r)^2 \rangle^{3/2}} \tag{8}$$

where $\langle . \rangle$ stands for space average. $S(r)$ is shown in the inset of figure 4.

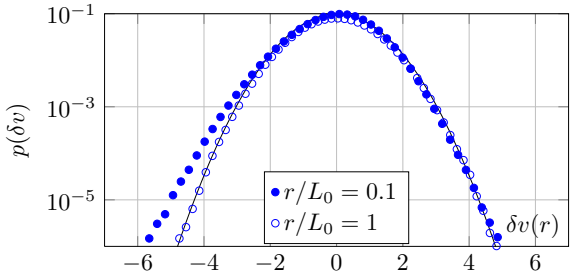

Fig. 3: Experimental histogram of the longitudinal velocity increments at large and intermediate scales in a superfluid turbulent flow ($T = 1.56\,\mathrm{K}$). Solid black line: Gaussian PDF.

Above the superfluid transition, $S(r)$ is known to be linked to the transfer rate (or flux) of the energy cascade [22]. Its value at our smallest resolved scale is fairly compatible with the values (close to -0.23) already reported in the literature (in the limit of vanishing scale r); a review of experimental values for $208 \leq R_\lambda \leq 2500$ may be found in [23]. The negative sign of $S(r)$ is a direct evidence that energy cascades from large to small scales.

Below the superfluid transition, the value of the skewness is found nearly identical to the value above the superfluid transition. This is a strong hint that energy cascades in a similar fashion above and below the superfluid transition. More quantitatively, in classical homogeneous and isotropic turbulence, the 4/5-law states that

$$\langle \delta v(r)^3 \rangle = -\frac{4}{5}\epsilon r \tag{9}$$

where ϵ stands for the mean dissipation rate of kinetic energy. This equation is only valid for inertial scales r, at which cascade dynamics prevails. It is often cited as the only exact result of classical fully-developed turbulence, *i.e.* for asymptotically large Re. It is our motivation to test its validity in quantum turbulence. In our experimental setting $R_\lambda \approx 1640$ and, therefore, Eq. 9 is expected to be "approached" in a finite inertial range of scales [24].

In order to compare superfluid experimental data to this classical prediction, ϵ needs to be estimated at first. Getting an accurate estimate of ϵ from experimental data is not trivial. A common practice is to use the third-order structure function and assume the 4/5-law. This method is known to yield reasonable estimates of ϵ for $R_\lambda \gtrsim 1000$ [25, 26]. Since our aim is here to assess the 4/5-law, we can not use this method directly. However, previous experiments have shown that ϵ does not change when the superfluid transition is crossed (keeping the same mean-flow velocity above and below the transition) [15]. Therefore, we have estimated ϵ from the 4/5-law using He I velocity recordings — where it is known to hold, since He I is a classical fluid — and then used that estimate to compensate the third-order velocity structure function obtained in He II. We have obtained $\epsilon = 5.4(3) \times 10^{-3}\,\mathrm{m^2/s^3}$.

We observe a "plateau" for nearly half a decade of scales, corresponding to the resolved inertial range of the turbulent cascade (see figure 4). The value of this "plateau" is comparable above and below the superfluid transition, within an experimental uncertainty of about 25 %. This may be viewed as the first experimental evidence that the 4/5-law (Eq. 9) remains valid in superfluid turbulence, at least at the largest inertial scales.

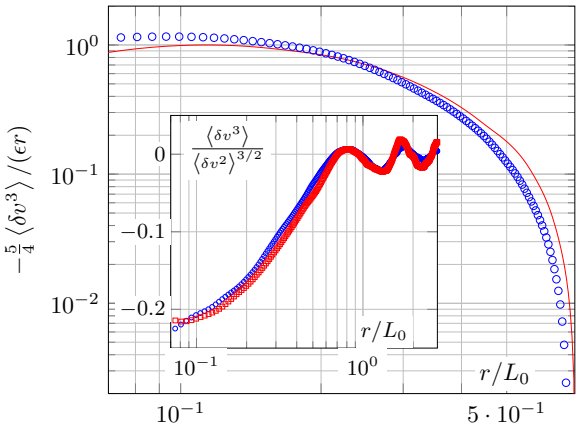

Fig. 4: Experimental third-order velocity structure function compensated by the 4/5-law (Eq. 9) obtained in superfluid helium at $T = 1.56\,\mathrm{K}$ (blue circles) and in classical liquid helium at $T = 2.2\,\mathrm{K}$ (red squares). Inset: Skewness of the distribution of longitudinal velocity increments (same color code). The smallest abscissa $r/L_0 = 7 \times 10^{-2}$ corresponds to the probe cut-off. The oscillation at large scales is related to the frequency of the vortex shedding.

Direct numerical simulations. – In this section, we examine turbulent velocity fields obtained from a pseudo-spectral simulation of He II dynamics in a cubic box (with resolution 512^3–1024^3 and periodic boundary conditions). Stationarity is ensured by an isotropic external force acting at some large scale L_0. The numerical procedure is detailed in [20]. The dynamical equations write as

$$\frac{D\vec{v}_n}{Dt} = -\frac{1}{\rho_n}\nabla p_n + \frac{\rho_s}{\rho}\vec{F}_{ns} + \frac{\mu}{\rho_n}\nabla^2\vec{v}_n + \vec{f}_n^{ext} \tag{10}$$

$$\frac{D\vec{v}_s}{Dt} = -\frac{1}{\rho_s}\nabla p_s - \frac{\rho_n}{\rho}\vec{F}_{ns} + \vec{f}_s^{ext} \tag{11}$$

where indices n and s refer to the normal and superfluid components, respectively; $\vec{f}_n^{ext}$ and $\vec{f}_s^{ext}$ are external (divergence-free) forces; μ is the dynamic viscosity. The mutual coupling force is approximated by its first-order expression:

$$\vec{F}_{ns} = -\frac{B}{2}\left|\vec{\omega}_s\right|\left(\vec{v}_n - \vec{v}_s\right) \tag{12}$$

where $\vec{\omega}_s = \nabla\times\vec{v}_s$ is the superfluid vorticity and $B = 2$ is taken as the mutual friction coefficient [27]. The normal and superfluid velocity fields are assumed incompressible, *i.e.* $\nabla\cdot\vec{v}_s = \nabla\cdot\vec{v}_n = 0$.

In our simulations, we fix the cut-off resolution at the value of the mean quantum inter-vortex distance, δ. This latter is estimated from the quantum of circulation, κ, around a single superfluid vortex and from the average vorticity,

$$\delta^2 = \frac{\kappa}{\sqrt{\left\langle\left|\vec{\omega}_s\right|^2\right\rangle}} \tag{13}$$

This truncation procedure was validated by the accurate prediction of the vortex line density in experiments [20].

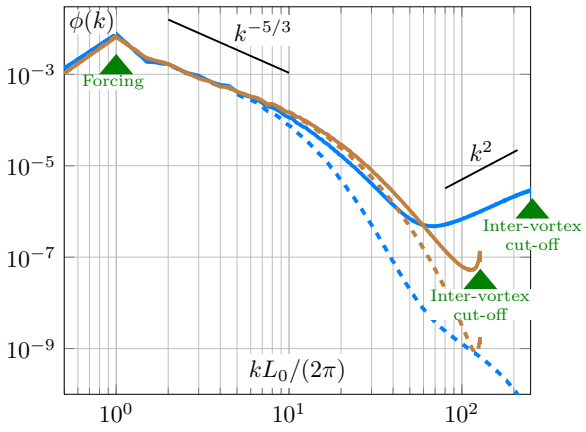

Fig. 5: Simulated 3D velocity power spectra. Solid lines are obtained from the velocity field of the superfluid component, $\vec{v}_s$. Dashed lines are obtained from the velocity field of the normal component, $\vec{v}_n$. The sky blue spectra were obtained at very low temperature ($T = 1.15\,\mathrm{K}$, 1024^3) ; the chocolate spectra were obtained at high temperature ($T = 2.1565\,\mathrm{K}$, 512^3). The smallest resolved scale matches the inter-vortex spacing. L_0 is defined as the forcing scale.

The velocity power spectra for normal and superfluid components are displayed in figure 5 in the very-low-temperature and high-temperature limits: $T = 1.15\,\mathrm{K}$ and $T = 2.1565\,\mathrm{K}$ corresponding to $\rho_s/\rho_n = 40$ and $\rho_s/\rho_s = 0.1$, respectively. In order to allow closer comparisons with experiments, the Reynolds number Re is estimated as

$$Re = \frac{L_0\sqrt{\langle v_m^2\rangle}}{\mu/\rho} \tag{14}$$

where $v_m = \left(\rho_n v_n + \rho_s v_s\right)/\rho$ is the momentum velocity[2], $L_0 = \pi$ is the length-scale corresponding to the forcing wave-number $k_0 = 1$ and μ/ρ is the kinematic viscosity. The power spectrum of the momentum velocity is not plotted but nearly matches the normal-component spectrum at high temperature and the superfluid-component spectrum at very low temperature, as expected from the mass density ratio.

The very-low-temperature and high-temperature simulations have nearly the same Reynolds number: $Re = 1960$ and $Re = 2280$ respectively, which are much smaller than the Reynolds number of the experiment: $Re = 1.8\times10^5$. Yet, in both cases, the spectra collapse at large scales close to a Kolmogorov's $k^{-5/3}$ scaling but differ at smaller scales, named "meso-scales" [20]. In this range of meso-scales, larger than the inter-vortex scale but smaller than inertial scales, the superfluid component is no longer locked to the normal component. At the lowest temperatures, its energy distribution approaches a k^2 scaling, as evidenced in figure 5, which is compatible with the equipartition of superfluid energy.

The momentum velocity third-order longitudinal structure function is estimated by averaging the longitudinal increment along the three directions in one "snapshot" of the flow[3]. One does not expect the 4/5-law to hold exactly at such moderate Reynolds number, discrepancies being related to the viscous dissipation (at small scales) and the external forcing (at large scales) [24]. However, we observe at high temperature that (i) the compensated third-order structure function reaches a maximum slightly lower than one, which is consistent with reported observations in classical turbulence (at comparable Reynolds numbers) [26], and (ii) the small-scale behavior goes typically like r^2 corresponding to the continuous (or smooth) limit $\delta u(r) \sim r$. At very low temperature, the velocity field is no longer smooth at very small scales. It exhibits irregular fluctuations, down to the smallest scales, related to the equipartition noise. This yields a different behavior of $\langle\delta v(r)^3\rangle$ as shown in figure 6. It is important to mention that the (total) disssipation rate, ϵ, is eventually a parameter of our simulations. Indeed, $\rho\epsilon$ equals the power

[2]We used the one-dimensional rms value, $v_{\mathrm{rms,1d}} = v_{\mathrm{rms,3d}}/\sqrt{3}$ to be comparable with experiments.

[3]We obtain similar results if the velocity increments are computed with the velocity field from the dominant component rather than v_m. The momentum velocity is convenient because it is defined for all temperatures and comparable to what is measured in experiments.

of the external forces (by assuming stationarity). This injected power is fixed and kept constant in our numerical scheme [20].

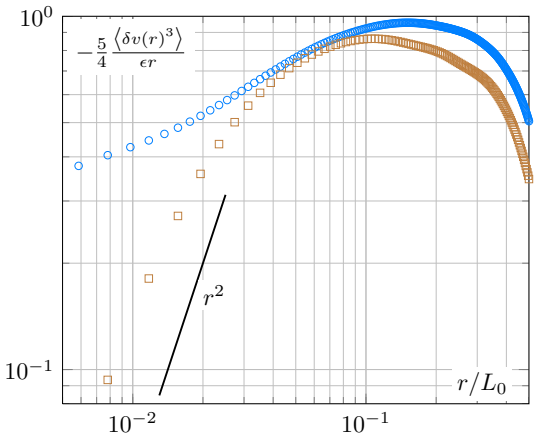

Fig. 6: Compensated third-order structure function obtained in numerical simulations at high temperature (chocolate squares) and very low temperature (sky blue circles) for nearly the same Reynolds numbers.

In the following, we address the departure from the ideal 4/5-law at small scales, *i.e.* related to the viscous dissipation. Let us mention that departure at large scales (related to the external forcing) is beyond the scope of the present study and does not spoil the present results.

In classical turbulence, the viscous dissipation is accounted in the Kármán-Howarth equation, which generalizes the 4/5-law at small scales:

$$\langle \delta v(r)^3 \rangle + \frac{4}{5}\epsilon r = 6\nu \frac{\mathrm{d}\langle \delta v(r)^2 \rangle}{\mathrm{d}r} \qquad (15)$$

This Kármán-Howarth equation can be interpreted as an exact scale-by-scale energy budget. Physically, the right-hand side of Eq. 15 takes into account the energy that leaks out of the cascade due to the viscous dissipation. Such generalization applied to the two-fluid model contains a term associated with the mutual friction between the superfluid and normal components, which can not be formulated (strictly speaking) into a form similar to Eq. 15. However, we propose here to pursue an empirical approach and assess to what extent the classical relation (Eq. 15) can be applied to He II. Formally, an effective kinematic viscosity can be defined from the deviation to the 4/5-law at small scales. More precisely, let us introduce

$$\mathcal{N}(r) = \frac{\langle \delta v^3 \rangle + \frac{4}{5}\epsilon r}{6\frac{\mathrm{d}\langle \delta v^2 \rangle}{\mathrm{d}r}} \qquad (16)$$

For a classical Navier-Stokes fluid, Eq.15 implies that $\mathcal{N}(r)$ should match the kinetic viscosity μ/ρ from the "center" of the inertial range down to the smallest scales.

The values of $\mathcal{N}(r)$, normalized by μ/ρ, are plotted versus scale in figure 7. For all simulated temperatures, ranging from $T = 1.15\,\mathrm{K}$ ($\rho_s/\rho_n = 40$) to $T = 2.1565\,\mathrm{K}$

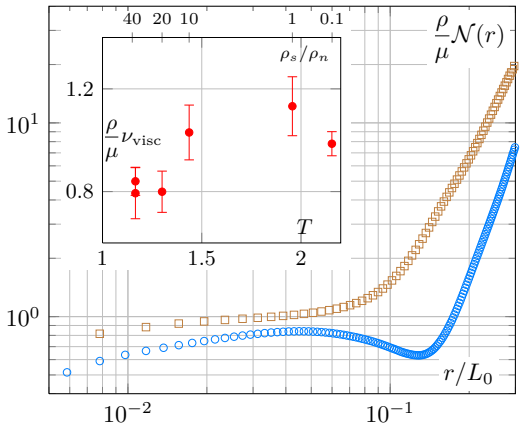

Fig. 7: Compensated effective viscosity versus scale obtained in numerical simulations at high temperature (chocolate squares) and very low temperature (sky blue circles) for nearly the same Reynolds number. Inset: effective viscosity estimated from the "plateau" of $\mathcal{N}(r)$ for various temperatures.

($\rho_s/\rho_n = 0.1$), this plot exhibits a "plateau" in the inertial range, quite analogous to what is expected for a classical fluid. This means that the deviation to the 4/5-law can be described (at first approximation) by introducing a constant effective viscosity. Interestingly, this remains valid even at very low temperatures, where the density of the normal component is also very small. This implies that the mutual friction term in the superfluid equation (Eq. 11) cannot be neglected at very low temperature (even if it is proportional to $\rho_n/\rho \ll 1$) and that it mimics to some extent a "viscous leak" along the cascade. Nevertheless, $\mathcal{N}(r)$ deviates from the plateau at the smallest scales, where both components are no longer locked, especially at very low temperature (sky blue circles). This is in contrast with classical turbulence, for which the "plateau" would extend down to the smallest scales [25].

From the "plateau"-value of $\mathcal{N}(r)$, we define the effective viscosity ν_{visc}. The estimates of ν_{visc} (compensated by μ/ρ) for various temperature and Reynolds-number conditions are gathered in the inset of figure 7. It is remarkable that this effective viscosity matches the dynamic viscosity of the normal component (normalized by the total density) within 20 % for all temperatures. As a result, these simulations indicate that superfluid helium (He II) behaves roughly as a viscous fluid at scales for which both normal and superfluid components are nearly locked, *i.e.* along the energy cascade. Furthermore, this feature remains satisfied at the lowest temperatures, where the normal (viscous) component fraction is smaller than 3 %.

Concluding remarks. – Using third-order longitudinal velocity structure functions, we have argued both experimentally and numerically that (stationary) turbulence in superfluid helium is consistent with an energy cascade in the sense of Kolmogorov's theory. In particular, our experimental data are quantitatively compatible

with the classical 4/5-law in the inertial range. It is worth pointing out that structure functions have been analyzed in the usual way because vortex singularities of the superfluid have been smoothed out, either by the large-size (compared with the inter-vortex distance) probe or by the coarse-grained resolution of the simulation model. Without this low-pass filtering of the details of the superfluid vortex tangle, comparisons with classical turbulence would have been less straightforward.

The "energy leak" from the cascade was assessed by applying the Kármán-Howarth equation on simulated velocity fields. We find that He II behaves as a viscous fluid in its cascade range with an effective viscosity, $\nu_{\rm visc}$, inherited from the normal component, even down to the lowest temperature ($\rho_s/\rho_n = 40$). This conclusion does not extent down to the smallest (meso)-scales when both components are unlocked and quasi-equipartition is evidenced. It is interesting to compare $\nu_{\rm visc}$ with an (other) effective viscosity, $\nu_{\rm eff}$, defined in the literature as [3]

$$\epsilon = \nu_{\rm eff}\left(\frac{\kappa}{\delta^2}\right)^2 \simeq \nu_{\rm eff}\left|\omega_s\right|^2 \qquad (17)$$

These two viscosities are comparable at high temperature [8], which can be understood by writing that both normal and superfluid components are roughly locked down to the (viscous) dissipation length scale:

$$\nu_{\rm eff} \equiv \epsilon\left|\omega_s\right|^{-2} \simeq \epsilon\left|\omega_n\right|^{-2} = \frac{\mu}{\rho_n} \simeq \frac{\mu}{\rho} = \nu_{\rm visc} \qquad (18)$$

However, $\nu_{\rm eff}$ departs from the "viscous viscosity", $\nu_{\rm visc}$, as the temperature is lowered [8–10], but becomes compatible with the "friction viscosity", $\nu_{\rm frict} = \kappa\frac{\rho_n B}{2\rho}$. This latter viscosity can be derived from Eqs. 10 and 11 assuming that both components are unlocked at small scales, which entails dissipation by friction of one fluid component on the other [28] (see [3] for a microscopic derivation). Thus, the definition of $\nu_{\rm eff}$ encompasses the two dissipative mechanisms occuring in He II at finite temperature ($T \geq 1\,{\rm K}$), *i.e.* the "viscous dissipation", $\nu_{\rm visc}$, that we discuss in this letter, and the "friction dissipation", $\nu_{\rm frict}$. It would be interesting to understand how $\nu_{\rm eff}$ (Eq. 17) depends on the relative weight of the two dissipation mechanisms and on a third dissipation mechanism relevant in the zero temperature limit: sound emission by vortex line [29–31]. The analytical integration of the Kármán-Howarth for the two-fluid model, which implies additional modeling, would open this perspective.

As a perspective to further understand the mechanisms leading to viscous-like behavior, we point out a possible analogy with classical truncated Euler systems, in which the presence of an equipartitioned reservoir at small scales acts as a molecular viscosity at larger scales [32–34].

Acknowledgments. – This work benefited from the support of ANR (ANR-09-BLAN-0094) and from the computing facilities of PSMN at ENS Lyon and of GENCI-CINES (grant 2011-026380). We are grateful to Grégory Garde who designed and built the Helium wind tunnel and to Pierre Chanthib, Étienne Ghiringhelli, Pierre-Luc Delafin, Jacques Depont and Jean-Luc Kueny for their help. We thank Laurent Chevillard, Yves Gagne, Bernard Castaing and Roberto Benzi for interesting discussions.

REFERENCES

[1] Kolmogorov A., *C. R. Acad. Sci. USSR* , **30** (1941) 301-305.
[2] Landau L., *Phys. Rev.* , **60** (1941) 356.
[3] Vinen W. F. and Niemela J. J., *J. Low Temp. Phys.* , **128** (2002) 167.
[4] Sergeev Y., *Nature Physics* , **7** (2011) 451.
[5] Roche P.-E. *et al.*, *EPL* , **77** (2007) 66002.
[6] Bradley D. *et al.*, *Phys. Rev. Lett.* , **101** (2008) 065302.
[7] Stalp S. R., Skrbek L. and Donnelly R. J., *Phys. Rev. Lett.* , **82** (1999) 4831.
[8] Niemela J., Sreenivasan K. and Donnelly R., *J. Low Temp. Phys.* , **138** (2005) 537.
[9] Chagovets T., Gordeev A. and Skrbek L., *Phys. Rev. E* , **76** (2007) 027301.
[10] Walmsley P. and Golov A., *Phys. Rev. Lett.* , **100** (2008) 245301.
[11] Rousset B. *et al.*, in proc. of *15th Int. Cryo. Eng. Conf.* Cryogenics, Vol. 34 Supplement 1, 1994 pp. 317–320.
[12] Smith M. R., Hilton D. K. and Sciver S. W. V., *Phys. fluids* , **11** (1999) 751.
[13] Fuzier S. *et al.*, *Cryogenics* , **41** (2001) 453.
[14] Maurer J. and Tabeling P., *EPL* , **43** (1998) 29.
[15] Salort J. *et al.*, *Phys. fluids* , **22** (2010) 125102.
[16] Benzi R., in *Classical and Quantum Turbulence Workshop, Abu Dhabi*, May 2nd, 2011.
[17] Samuels D. C. and Kivotides D., *Phys. Rev. Lett.* , **83** (1999) 5306.
[18] Donnelly R. and Barenghi C., *J. Phys. Chem. Ref. Data* , **27** (1998) 1217.
[19] Kivotides D. *et al.*, *EPL* , **57** (2002) 845.
[20] Salort J. *et al.*, *EPL* , **94** (2011) 24001.
[21] Pinton J.-F. and Labbé R., *J. Phys. II* , **4** (1994) 1461.
[22] Monin A. and Yaglom A., *Statistical Fluid Mechanics* (MIT Press, Cambridge) 1971.
[23] Chevillard L. *et al.*, *Physica D* , **218** (2006) 77.
[24] Antonia R. A. and Burattini P., *J. Fluid Mech.* , **550** (2006) 175.
[25] Moisy F. *et al.*, *Phys. Rev. Lett.* , **82** (1999) 3994.
[26] Ishihara T. *et al.*, *Annu. Rev. Fluid Mech.* , **41** (2009) 165.
[27] Barenghi C. and Donnelly R., *J. Low Temp. Phys.* , **52** (1983) 189.
[28] Roche P.-E. *et al.*, *EPL* , **87** (2009) 54006.
[29] Nore C. *et al.*, *Phys. Rev. Lett.*, **78** (1997) 3896.
[30] Vinen W., *Phys. Rev. B* , **61** (2000) 1410.
[31] Leadbeater M. *et al.*,*Phys. Rev. Lett.* , **86** (2001) 1410.
[32] Kraichnan R. and Chen S., *Physica D* , **37** (1989) 160.
[33] Cichowlas C. *et al.*, *Phys. Rev. Lett.* , **95** (2005) 264502.
[34] Bos W. and Bertoglio J.-P., *Phys. fluids* , **18** (2006) 071701.